GEOPHYSICAL RESEARCH LETTERS, VOL. 27, NO. 3, PAGES 433-436, FEBRUARY 1, 2000

Wave-guide effects in subduction zones: evidence from three-dimensional modeling

N.M. Shapiro[1], K. B. Olsen[2], and S.K. Singh[1]

Abstract. We have simulated seismic wave propagation in models of the subduction zone off the Pacific coast of Mexico using a three-dimensional finite difference method. The results show that a significant part of the energy generated by earthquakes in the subduction zone can be trapped inside a wave-guide generated by the low-velocity material of the accretionary prism. The trapped waves in the simulations appear as long-duration wave-trains that follow the onset of the surface waves, similar to the signature of broadband seismograms recorded by stations along the Pacific coast of Mexico for subduction earthquakes.

Introduction

Subduction zones represent one of the most prominent tectonic features of the earth. Within these zones of convergence between the oceanic and the continental plates some of the largest earthquakes in any tectonic regime take place, e.g., the 1960, Chile (moment magnitude (M_W = 9.5) and the 1964, Alaska (M_W = 9.2) earthquakes. The study of these earthquakes is very important for our understanding of the geodynamical processes in subduction zones and for the estimation of seismic hazard in the coastal areas of many Pacific countries.

Seismic radiation from subduction zone earthquakes can be strongly affected by the heterogeneity in the source region. In particular, low velocity layers tend to promote the entrapment of seismic energy, resulting in coda-type phases with relative long duration and large amplitude. For example, quasi-monochromatic waves with such characteristics following teleseismic P phases from large earthquakes in the Chilean subduction zone have been interpreted as entrapment of compressional waves in the water layer [*Ihmlé and Madariaga*, 1996]. Seismic waves trapped in the low-velocity zone formed by untransformed oceanic crust have been observed in Japan [*Hori et al.*, 1985]. The accretionary prism is another low-velocity structure possibly significantly affecting the wavefield generated by subduction-zone earthquakes [*Shapiro et al.*, 1998]. Analysis of ground motions recorded by stations located close to the Pacific coast of Mexico showed two significant long-period (6-30 s) phases in the records: a Rayleigh wave propagating in the continental plate, followed by a phase with duration in excess of 100 s at some stations. The latter has been interpreted as a wave trapped in the accretionary prism by mechanisms similar to those responsible for extended durations of earthquake ground motions in sedimentary basins [*Olsen et al.*, 1995] and fault zones [*Ben-Zion and Aki*, 1990; *Li et al.*, 1990].

Numerical Method and Subduction Zone Models

The crustal structure of subduction zones are typically characterized by significant heterogeneity as a result of the prevailing compressional tectonic processes (Figure 1). For example, the seismic velocities of the oceanic crust are generally larger than those in the overriding continental crust. However, the largest variation of elastic parameters is believed to be caused by the accretionary prism, the wedge-shaped accumulation of sediments scraped off the subducting plate and exposed to immense tectonic forces. This prism is typically composed of a few kilometers of very soft material and generates a strong contrast in seismic velocities relative to the surrounding crust.

Traditionally, studies of earthquakes and the resulting ground motion in subduction zones have used very simplified crustal models, such as 1D velocity structures [*Campillo et al.*, 1989] or semiempirical modeling [*Ordaz et al.*, 1995]. Such simplification of the models eliminates effects from wave entrapment and surface wave-generation at lateral discontinuities and may therefore lead to significant errors in estimation of source and ground motion parameters. A recent study included 2D and 3D heterogeneous crustal models to simulate ground motion from earthquakes in the Mexican

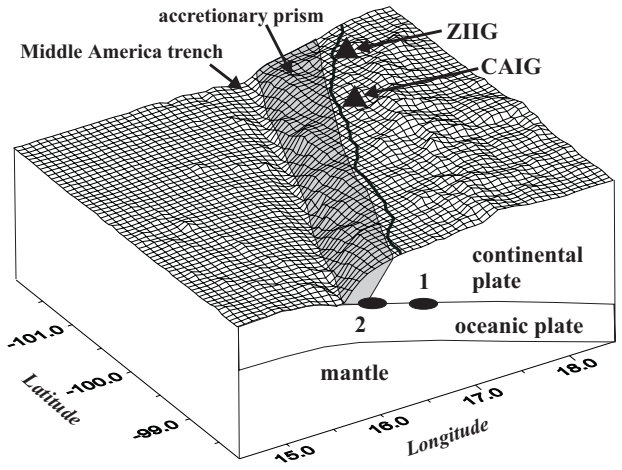

Figure 1. 3D schematic perspective showing the bathymetry of the Mexican subduction zone. Triangles depict the locations of stations where we compare data with finite-difference synthetics for events 1 and 2 (hypocenters depicted by ellipses).

[1]Instituto de Geofísica, Universidad National Autónoma de México, México D.F., Mexico
[2]Institute for Crustal Studies, University of California at Santa Barbara, USA

Paper number 1999GL010982.
0094-8276/00/1999GL010982$05.00

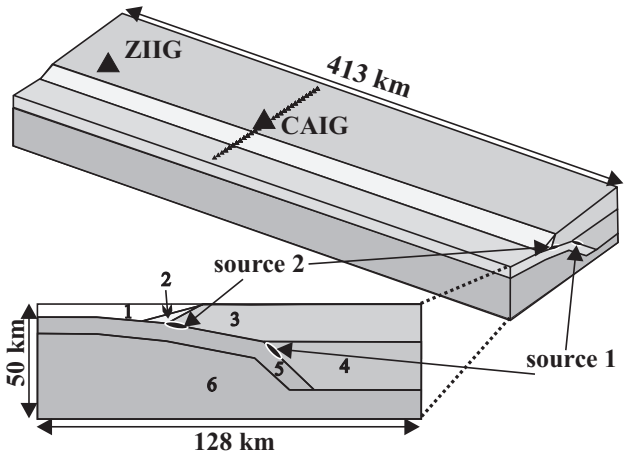

Figure 2. 3D model used in the finite-difference simulations.The two large triangles depict the locations of stations where data was compared with finite-difference synthetics for events 1 and 2 (hypocenters depicted by ellipses). Small triangles depict the location of stations used for analysis of the wave propagation. The numbers correspond to the model layers defined in Table 1.

subduction zone [*Furumura and Kennett*, 1998]. However, their models did not include the accretionary prism.

More accurately, a subduction zone can be represented as a two-and-a-half dimensional (2.5D) structure, with the structure varying laterally only perpendicular to the trench. Figure 2 and Table 2 show such 2.5D model for the area off the subduction zone along the Pacific coast of Mexico, with the geometry, velocities, and densities constrained by gravity and seismic data[*Kostglodov et al.*, 1996].

We use the crustal model shown in Figure 2 and a staggered-grid finite-difference method to test whether numerical simulations of wave propagation can reproduce the long-period coda observed in seismic data recorded along the Mexican subduction zone. We simulate two events (Figure 2, Table 2), one with epicenter located on-shore 60 km from the trench (source 1), and another located near the continental edge of the accretionary prism (source 2). The fourth-order accurate implementation of the finite-difference method used here has proved to be an efficient tool for 3D numerical wave propagation in large-scale earth models [*Olsen*, 1994; *Olsen et al.*, 1995].

The ruptures are kinematically simulated radially propagating outward with a constant velocity and slip. Due to the simplified geometry of the 2.5D model we approximate the focal mechanisms of the earthquakes with purely thrust mechanisms, strike parallel to the trench and dip according to the slope of the oceanic crust at the source insertion (Figure 2). We use an isosceles triangular slip rate function with rise time and fault area of 1 s and 8 km by 11 km, respectively, for source 1, and 2 s and 11 km by 11 km, respectively, for source 2. The source is implemented in the finite-difference grid by adding $-M_{ij}/V$ to S_{ij}, where M_{ij} is the ijth component of the moment tensor for the earthquake, $V = dx^3$ is the cell volume, and S_{ij} is the ijth component of

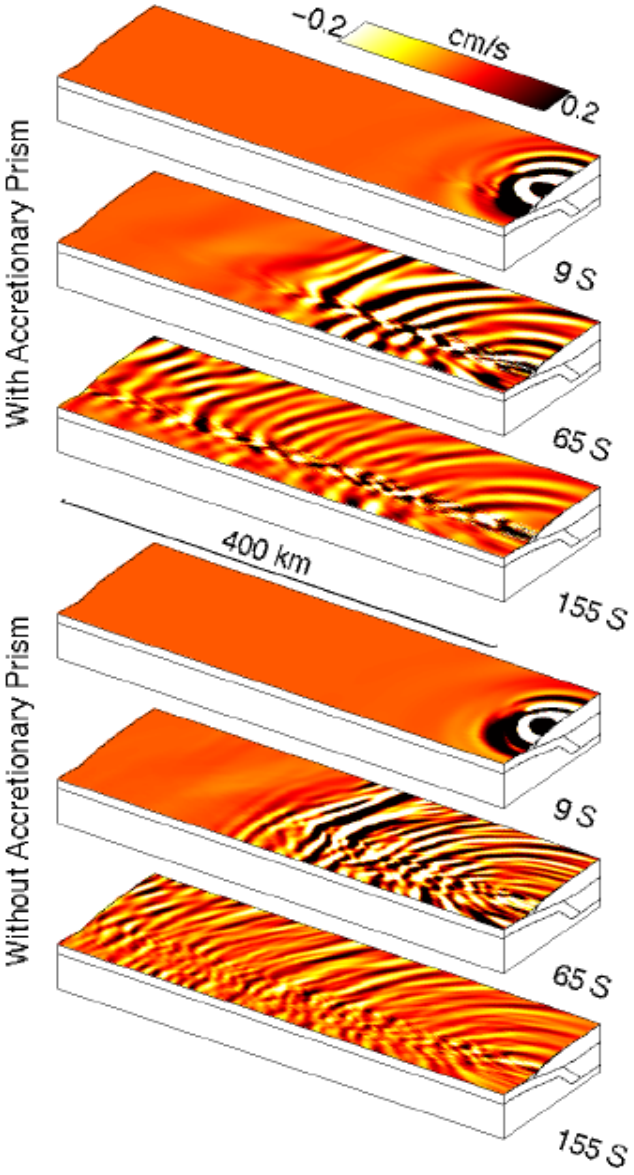

Figure 3. Snapshots of the wave propagation at three instants of time for the simulations with (top) and without (bottom) the accretionary prism for source 1 (Figure 1 and 2). All snapshots are scaled by the factor used for the synthetics associated with source 1 in Figure 5.

Table 1. Layers included in the models: (1) water, (2) the accretionary prism, (3) the upper continental crust, (4) the lower continental crust, (5) the oceanic crust, and (6) the upper mantle.

N	ρ (g/cm^3)	V_P (km/s)	V_S (km/s)
1	1.0	1.5	0
2	2.1	2.8	1.5
3	2.7	5.9	3.4
4	3.0	6.5	3.75
5	2.9	6.75	3.9
6	3.3	7.8	4.5

Table 2. Source Parameters.

N	yy.mm.dd	Lat	Lon	H (km)	M_w
1	96.03.27	16.4	-98.2	20	5.5
2	97.07.19	16.0	-98.2	10	6.7

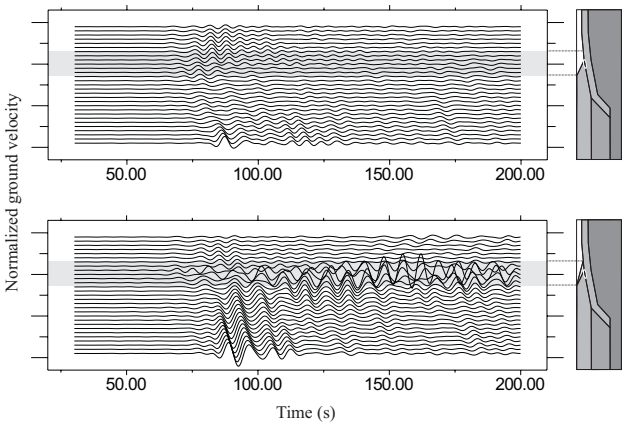

Figure 4. Comparison of synthetic seismograms along a profile perpendicular to the subduction zone (Figure 2) computed in models with (top) and without (bottom) the accretionary prism. All traces are scaled by a common factor.

the stress tensor on the fault at time t. Absorbing boundary conditions [*Clayton and Engquist*, 1977] are applied to the sides of the computational model. To further reduce artificial reflections the boundaries of the model are padded with a zone of attenuative material [*Cerjan et al.*, 1985]. The 3D modeling parameters are listed in Table 3.

Analysis of Numerical Simulations

We present all our numerical simulations in the following at the water-solid and solid-air interfaces. The water-solid interface was selected rather than the water-air interface in order to evaluate the seismic response on the surface of the accretionary prism. All synthetics and data are presented as vertical-component particle velocities, bandpass filtered

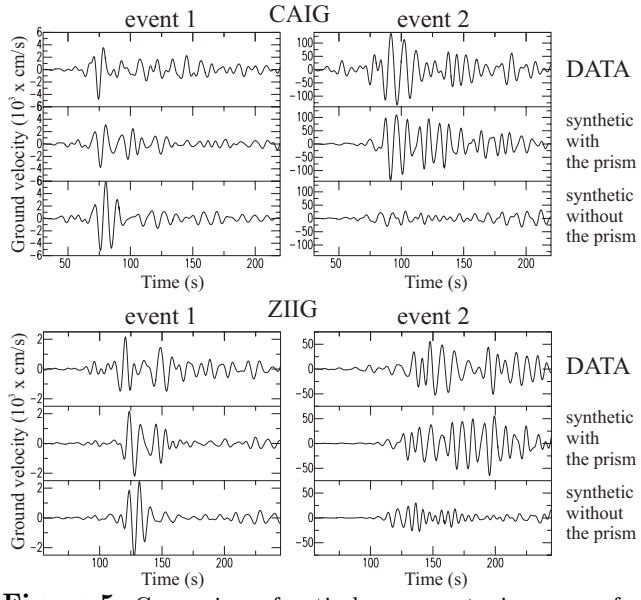

Figure 5. Comparison of vertical-component seismograms for (top) data, (middle) synthetics for the model including and (bottom) excluding the accretionary prism at stations CAIG and ZIIG for events 1 and 2 (Figure 1 and 2). For a given station and event, the synthetic traces are scaled by a common factor.

Table 3. 3-D Modeling Parameters.

Spatial discretization (m)	750
Temporal discretization (s)	0.043
Grid points along trench	600
Grid points perpendicular to trench	226
Grid points along vertical	70

to frequencies between 0.06 and 0.2 Hz. A commonly used rule of thumb requires 5 points per minimum wavelength for accurate wave propagation using a fourth-order accurate scheme [*Levander*, 1988]. However, it is possible that the strong impedance contrast between the water layer and the accretionary prism in our model as well as an abundance of surface waves with relatively slow propagation velocities may introduce an unacceptable amount of numerical dispersion in the results, even when this criteria is met. For these reasons we honor at least 10 points per minimum shear wavelength. Since the depth extent of our model is limited (40 km), our simulations do not include the extremely long wavelengths of the surface waves traveling in the mantle. We therefore highpass filter our synthetics at 0.06 s.

Figure 3 shows a comparison of snapshots for simulations in models with and without the accretionary prism using source 1. Clearly, the wave propagation in the two models are quite different. At 9 s, seismic energy starts to be transferred from the continental and oceanic crust into the accretionary prism. At 65 and 155 s, the snapshots for the simulations in the model including the accretionary prism show a substantial amount of energy propagating inside the accretionary prism. The slightly perturbed wavefield in this area for the model without the prism is caused by the strong impedance contrast at the intersection between the water layer and the continental and oceanic crusts.

In Figure 4 we show the effect of the accretionary prism for seismograms along a profile perpendicular to the trench (Figure 2). The seismograms calculated for the model including the accretionary prism and source 2 show a large-amplitude wave train with extended duration and amplitude above the trench. In the model without the accretionary prism, this wave train is practically absent. Note how the largest amplitude of the wave train occurs more than 150 s after rupture initiation. These results suggest that the long-duration wave-train corresponds to resonance of waves trapped in the accretionary prism.

To verify the importance of the prism as a wave-guide we compare our synthetic seismograms with observed broadband records from two stations, CAIG and ZIIG in Figure 5. CAIG is located 230 km from the estimated hypocenter of event 1, and the relative distance between the location of CAIG and ZIIG is 140 km along the trench (Figure 1 and 2). For both stations we compare data to synthetics computed for models with and without the accretionary prism for sources 1 and 2 (Figure 5). For event 1, both synthetic and observed signals are dominated by a relatively short-period arrival which is identified from its propagation velocity as a combination of Rayleigh and Love waves propagating in the continental crust [*Shapiro et al.*, 1998]. The initial phase is followed by a coda with amplitude at CAIG that is similar for the simulations calculated with and without the prism. However, at ZIIG, a strong phase arriving ~ 30

s after the surface wave is clearly distinguishable in both the data and synthetics calculated with the model including the accretionary prism, while it is absent in the synthetics calculated without the prism. For event 2, located close to the accretionary prism, the relative amplitude of the coda in the observed seismograms is much higher than that for event 1. In this case the direct surface wave cannot be separated from the coda, particularly at ZIIG. The synthetic seismograms calculated in the model including the accretionary prism reproduce the relative amplitude and coda duration reasonably well, while the coda is significantly reduced in the synthetics calculated without the accretionary prism. Based on the similarity between data and simulations we conclude that a large part of the seismic energy emitted by earthquakes with hypocenter locations close to the trench propagates along the subduction zone as waves trapped in the accretionary prism. As noticed in the data, the amplitude of the trapped waves in the simulations increase with decreasing hypocentral distance to the accretionary prism.

Discussion

We realize that our crustal model of the Mexican coast is somewhat poorly constrained and represent a simplification of the complexity present in a subduction zone. For example, our model does not include anelastic attenuation or small-scale heterogeneities in the geometry of the accretionary prism. However, synthetic tests that cannot be reported here indicate that neither the presence of the small-scale heterogeneities nor anelastic attenuation inside the accretionary prism significantly affect the amplitude or duration of the synthetic seismograms. Thus the model simplifications do not significantly affect the amplitude or duration of the trapped waves and, therefore, our conclusions that the presence of the low-velocity accretionary prism can strongly affect seismic wave propagation from nearby subduction zone earthquakes. It is possible that an improved fit could be obtained from trial-and-error refinement of the geometry of the subduction model but we leave this task for future work.

Acknowledgments. The computations in this study were partly carried out on SGI Origin 2000 computers at MRL, UCSB (NSF Grant CDA96-01954) and Los Alamos National Laboratories, with support from NSF Grant EAR 96-28682). We thank two anonymous reviewers for their advice leading to an improved manuscript. The work by N.M.S. and S.K.S. was supported by the DGAPA IN1095 98 project as well as the project FIES97-01-IV funded by Instituto Mexicano de Petróleo. Movies of the simulations can be found on the WWW at http://quake.crustal.ucsb.edu/∼kbolsen. This is ICS contribution # 00339-89EQ.

References

Ben-Zion, Y. and K. Aki Seismic radiation from an SH line source in a laterally heterogeneous planar fault zone, *Bull. Seism. Soc. Am. 90*, 971-994, 1990.

Campillo, M., J.C. Gariel, K. Aki, and F.J. Sanchez-Sesma, Destructive ground motion in Mexico City: source, path, and site effects during great 1985 Michoacan earthquake, *Bull. Seism. Soc. Am. 79*, 1718-1735, 1989.

Cerjan, C., D. Kosloff, R. Kosloff, and M. Reshef A nonreflecting boundary condition for discrete acoustic and elastic wave equations, *Geophysics 50*, 705-708, 1985.

Clayton, R. and B. Engquist, Absorbing boundary conditions for acoustic and elastic wave equations, *Bull. Seism. Soc. Am. 71*, 1529-1540, 1977.

Furumura, T. and B.L.N. Kennett, Anomalous surface waves associated with deep earthquakes, generated at an ocean ridge, *Geophys. J. Int. 134*, 134, 663-676, 1998.

Hori, S., H. Inoue, Y. Fukao, and M. Ukawa, Seismic detection of the untransformed 'basaltic' oceanic crust subducting into the mantle, *Geophys. J. R. Astr. Soc. 83*, 169-197, 1985.

Ihmlé, P.F. and R. Madariaga, Monochromatic body waves excited by great subduction zone earthquakes, *Geophys. Res. Lett. 23*, 2999-3002, 1996.

Kostglodov, V., W. Bandy, J. Dominguez, and M. Mena, Gravity and seismicity over the Guerrero seismic gap, Mexico, *Geophys. Res. Lett. 23*, 3385-3388, 1996.

Levander, A., Fourth-order finite-difference P-SV seismograms, *Geophysics 53*, 1425-1436, 1988.

Li, Y.-G., P.C. Leary, K. Aki, and P. Malin, Seismic trapped modes in the Oroville and San Andreas fault zones, *Science 249*, 763-766, 1990.

Olsen, K.B., Simulation of three-dimensional wave propagation in the Salt Lake Basin, *Ph.D. Thesis*, University of Utah, Salt Lake City, Utah, 157 p., 1994.

Olsen, K.B., R.J. Archuleta, and J.R. Matarese, Three-dimensional simulation of a magnitude 7.75 earthquake on the San Andreas fault, *Science 270*, 1628-1631, 1995.

Ordaz, M., J. Arboleda, and S.K. Singh, A scheme of random summation of an empirical Green's function to estimate ground motions from future large earthquakes, *Bull. Seism. Soc. Am. 85*, 1635-1647, 1995.

Shapiro, N.M., M. Campillo, S.K. Singh, and J. Pacheco, Seismic channel waves in the accretionary prism of the Middle America Trench, *Geophys. Res. Lett. 25*, 101-104, 1998.

N. Shapiro and S. Singh, Deportamento de Sismología y Volcanología, Instituto de Geofísica, UNAM, C.P. 04510, México, D.F., México. (email: shapiro@ollin.igeofcu.unam.mx)

K. Olsen, Institute for Crustal Studies, UC Santa Barbara, USA. (email: kbolsen@crustal.ucsb.edu)

(Received 08/06/1999; revised 09/20/1999;
accepted 09/23/1999.)